A Novel Boost Converter for Segmented-Stator Hybrid-Excitation Switched Reluctance Motor Drive with High Performance

Wen Ding, Shuai Yang and Yanfang Hu
School of Electrical Engineering, Xi'an Jiaotong University
Xi'an, China
wending@xjtu.edu.cn

***Abstract*—A novel boost converter with high performance is proposed to improve the dynamic characteristic of a 12/8-pole segmented-stator hybrid-excitation switched reluctance motor (SSHE-SRM) drive. The machine topology and static magnetic characteristics of the 12/8 SSHE-SRM are presented and compared with a conventional SRM (CSRM). The SSHE-SRM produces higher torque than CSRM, especially in the large current range. Thus, in order to increase the phase current of the SSHE-SRM under dynamic operation, the boost converter is employed. The operation states of the SSHE-SRM drive with the novel boost converter are analyzed in detail. During the fast-excitation and fast-demagnetization modes, phase voltage is boosted due to the addition of capacitor and hence faster-excitation and fast-demagnetization currents are obtained. Detailed simulations and experiments of the SSHE-SRM drive with this novel boost converter are carried out as well as compared with asymmetric half-bridge converter.**

Keywords—boost converter; high performance; segmented-stator hybrid-excitation switched reluctance motor

I. INTRODUCTION

Switched reluctance motors (SRMs) are attracting more and more interest in some variable speed drive applications. However, they also suffer from some disadvantages, such as low torque/power density, low efficiency, high torque ripple and acoustic noise when compared to permanent magnet (PM) machines.

In order to improve the system performances of SRMs, especially for higher torque production and density, lower torque ripple and higher efficiency, many studies have been investigated, which can be dived into two categories: one is focused on unique machine structures and another is focused on novel converters. For unique machine structures, the segmented-stator configuration is a good solution to improve the motor characteristics. A variety of segmented-stator SRMs, namely, C-core and E-core stator SRMs are proposed for low-cost production, wind power generation, fault tolerant drive system and EV applications in last decades [1-3]. They have been demonstrated to have higher torque production, higher efficiency, and lower weight than conventional SRM (CSRM).

On the other hand, apart from classical asymmetric half-bridge converter (AHBC), a lot of novel topologies of power converters have been proposed to improve the performance of SRM drives, typically including boost type converters, capacitor dump converters, R-dump, C-dump and passive boost converters, etc [4-8]. In these novel converters, some passive components, i.e., diode, capacitor and power switch are added and utilized.

Aside from these, hybrid-excitation with PMs is also a useful method to improve the characteristics of SRMs. Many different types of hybrid SRMs with PMs have been proposed to improve output torque, efficiency and power density [9-13]. In this paper, a 12/8-pole segmented-stator hybrid-excitation SRM (SSHE-SRM) with a novel boost converter (NBC) drive is proposed to boost the phase voltage and hence improve its dynamic performance. Detailed simulations and experiments of the SSHE-SRM drive with NBC are carried out as well as compared with AHBC.

II. MACHINE TOPOLOGY AND MAGNETIC CHARACTERISITCS

The machine topologies of 12/8 SSHE-SRM and CSRM with the same basic size are shown in Fig. 1. The stator of the SSHE-SRM is comprised of six segments. The PMs are embedded between two poles in each stator segment. There is neither yoke iron nor other ferromagnetic material between two adjacent C-core segments. The six C-shaped segments are evenly arranged along the rotor, which are characterized by their own independent magnetic structures. The flux generated by the PM is closed through the U-shaped segment and does not pass the rotor core and air gap. However, when the winding is excited with a current, the flux produced by excited coils and the flux produced by PM are added together. Both flux paths are in the same direction in the rotor tooth and air gap. Thus, the sum of magnetic fluxes will create a larger electromagnetic attraction force which is superior to that created by a normal electromagnet.

The static phase flux linkage and torque characteristics of the SSHE-SRM are shown in Fig. 2. As seen in Fig. 2, when all coils are not excited, the phase flux linkage of the SSHE-SRM created by the PM only at the aligned position is -0.1Wb. When the phase is excited under a small range, the total flux

This work was supported in part by the National Natural Science Foundation of China under Grant 51777161 and Grant 51477130.

linkage created by the excited-coil and PM is still negative. This is the main difference of the flux linkage between SSHE-SRM and CSRM.

Fig. 3 shows the average torque characteristics in the SSHE-SRM and CSRM for one half of electrical cycle. It can be seen that the SSHE-SRM produces higher torque than CSRM and the superiority becomes larger and larger with the current increases.

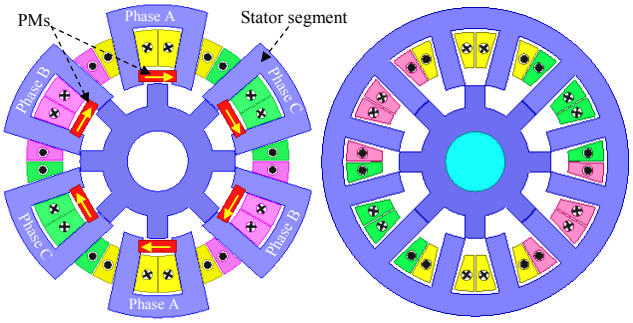

Fig. 1. Machine topologies of 12/8-pole (a) SSHE-SRM and (b) CSRM.

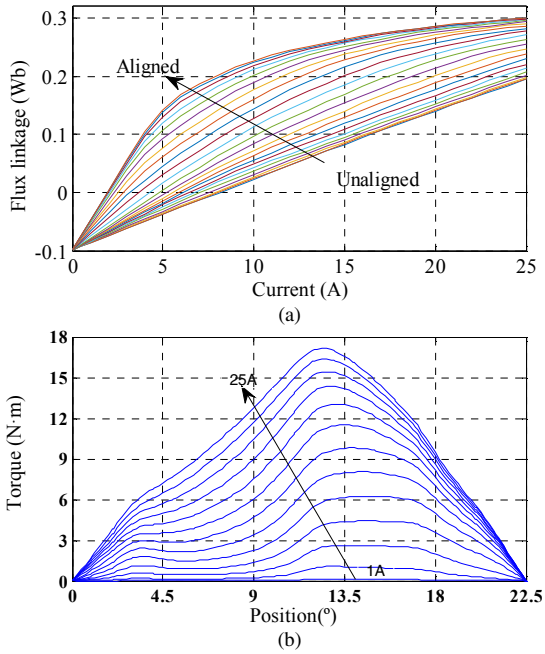

Fig. 2. Static magnetic characteristics of SSHE-SRM. (a) Phase flux linkage. (b) Static phase torque.

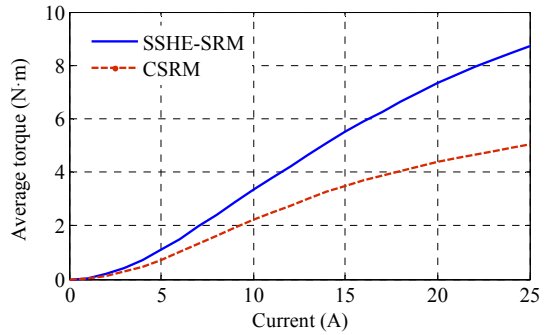

Fig. 3. Comparison of static average torque characteristic of two SRMs with different current densities.

III. Novel Boost Converter and Dynamicn Performance

As mentioned above, the SSHE-SRM appears to have higher torque production compared to CSRM, especially in the large current range. Thus, in order to increase the phase current of SSHE-SRM under dynamic operation, its power converter should be able to boost the voltage through the phase winding and to realize the rapid increase of winding current as well as increase the output torque of the motor. In this section, a novel boost converter (NBC) is employed to boost the phase voltage and hence to improve the dynamic perfromace of SSHE-SRM.

A. Topology of Novel Boost Converter

The topology of the NBC is shown in Fig. 4. Compared with asymmetric half-bridge converter (AHBC), four elements - a boost capacitor C_b, a power switch S_b and two diodes D_{b1} and D_{b2} are added in the boost converter. Thus, higher voltage can be applied to phase windings and fast excitation and fast demagnetization currents can be obtained owing to the addition of the capacitor voltage. The faster excitation and fast demagnetization can also improve the current tracing effect and hence improve the output torque performance.

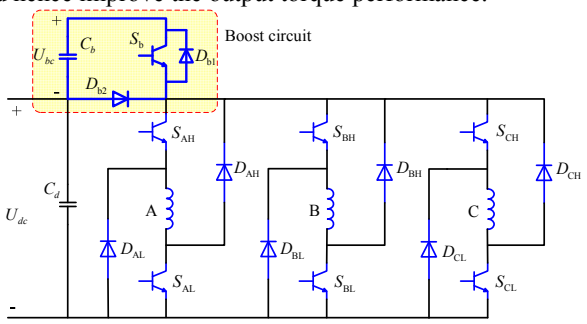

Fig. 4. The topology of the proposed novel boost converter (NBC).

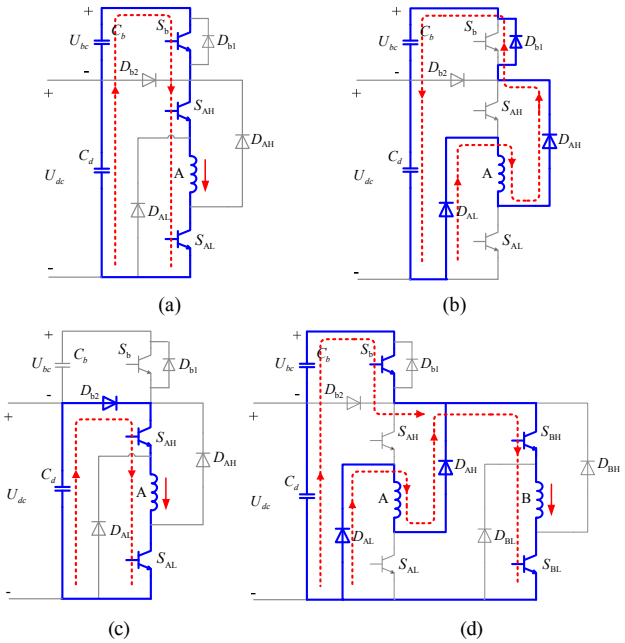

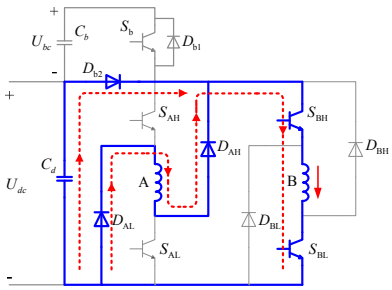

(e)

Fig. 5. Operation states of the SS-HESRM drive with the NBC. (a) State 1. (b) State 2. (c) State 3. (d) State 4. (e) State 5.

B. State Analysis of Novel Boost Converter

According to the relationship of the overlapping currents in the commutation region, the independent and effective operations of the SS-HESRM drive with the NBC can be divided into five states, as illustrated in Fig. 5.

1) State 1 (*Fast Excitation Mode*, *FEM*)

When all three switches S_b, S_{AH} and S_{AL} are turned on in one phase, the two capacitors- boost capacitor and dc-link capacitor are connected in series and a higher positive voltage is applied to the phase due to the additional capacitor voltage (U_{bc}). The phase will be excited with a greater current at a fast rate and a higher torque will be accordingly generated, which is called as fast excitation mode (FEM) and denoted as state 1. The phase is energised and the current flow path is shown in Fig. 5(a). The voltage and current equations of phase-A can be expressed as,

$$U_A = U_{dc} + U_{bc} = r \cdot i_A + \frac{d\psi_A(\theta, i_A)}{dt} \tag{1}$$

$$i_A = i_{dc} = i_{bc} \tag{2}$$

where U_{dc} and i_{dc} are the dc-link voltage and current, U_{bc} and i_{bc} are the boost capacitor voltage and current, r is the phase resistance, ψ_A is the total flux linkage in the excited phase-A and it can be described as,

$$\psi_A(\theta, i_A) = \psi_i(\theta, i_A) + \psi_{pm}(\theta, i_A) \tag{3}$$

where $\psi_i(\theta, i_A)$ is the flux linkage created by the excited phase-winding current, $\psi_{pm}(\theta, i)$ is the flux linkage created by the PM, which are both a function of the phase current and rotor position.

Thus, the voltage equation of the excited phase-A can be rewritten as,

$$U_A = U_{dc} + U_{bc} = r \cdot i_A + \frac{d\psi_i(\theta, i_A)}{dt} + \frac{d\psi_{pm}(\theta, i_A)}{dt} \tag{4}$$

2) State 2 (*Fast Demagnetization Mode*, *FDM*)

When all three switches S_b, S_{AH} and S_{AL} are turned off in one phase, the two capacitors- boost capacitor and dc-link capacitor are still connected in series; a higher negative voltage is applied to the phase. The energy stored in the phase is fed back to the dc-source supply. The current will go through D_{AH}, D_{AL} and D_{b1} and charge the boost capacitor C_b. Compared with ABHC, it can achieve faster demagnetization current with the torque decreasing quickly when the current is dropping, which is called as fast demagnetization mode (FDM) and denoted as state 2. The direction of current flow is presented in Fig. 5(b). The phase voltage and current equations can be expressed as (5) and (6).

$$U_A = -U_{dc} - U_{bc} = r \cdot i_A + \frac{d\psi_i(\theta, i_A)}{dt} + \frac{d\psi_{pm}(\theta, i_A)}{dt} \tag{5}$$

$$i_A = -i_{dc} = -i_{bc} \tag{6}$$

3) State 3 (*General Excitation Mode*, *GEM*)

When the additional switch S_b is turned off, and simultaneously S_{AH} and S_{AL} are turned on, the machine will excite a general current and torque, which is called as general excitation mode (GEM) and denoted as state 3. The phase is energised and the current flow path is similar to that of AHB converter, as shown in Fig. 5(c). The phase voltage equation can be expressed as (7).

$$U_{dc} = r \cdot i_A + \frac{d\psi_i(\theta, i_A)}{dt} + \frac{d\psi_{pm}(\theta, i_A)}{dt} \tag{7}$$

4) State 4 (*Two-Phase-Overlap Mode 1*)

According to the turn-on position of the incoming phase, the operation states of current overlap are divided into two cases, as shown in Fig. 5(d) and (e). In the first state, as shown in Fig. 5(d), the incoming phase-B is turned on, i.e., S_{BH}, S_{BL} and S_b are simultaneously turned on, before the fast demagnetization current of the outgoing phase-A is reduced to zero. The boost capacitor and dc-link capacitor are also connected in series, thus a higher negative voltage is applied to the outgoing phase-A and a higher positive voltage is applied to the incoming phase-B. In other words, the outgoing phase-A is in FDM and the incoming phase-B is in FEM.

In this case, the voltage and current equations of phase-A and phase-B can be expressed as (8)-(10).

$$U_A = -U_{dc} - U_{bc} = r \cdot i_A + \frac{d\psi_i(\theta, i_A)}{dt} + \frac{d\psi_{pm}(\theta, i_A)}{dt} \tag{8}$$

$$U_B = U_{dc} + U_{bc} = r \cdot i_B + \frac{d\psi_i(\theta, i_B)}{dt} + \frac{d\psi_{pm}(\theta, i_B)}{dt} \tag{9}$$

$$i_{dc} = i_{bc} = i_B - i_A \tag{10}$$

5) State 5 (*Two-Phase-Overlap Mode 2*)

In this state, as shown in Fig. 5(e), the additional switch S_b is turned off or the restored energy in the boost capacitor is reduced to zero, and the demagnetization current of the outgoing phase-A is not reduced to zero as well as the incoming phase-B is in GEM. The voltage and current equations of phase-A and -B can be expressed as (11)-(13).

$$U_A = -U_{dc} = r \cdot i_A + \frac{d\psi_i(\theta, i_A)}{dt} + \frac{d\psi_{pm}(\theta, i_A)}{dt} \tag{11}$$

$$U_B = U_{dc} = r \cdot i_B + \frac{d\psi_i(\theta, i_B)}{dt} + \frac{d\psi_{pm}(\theta, i_B)}{dt} \tag{12}$$

$$i_{dc} + i_A = i_B \tag{13}$$

From above five operation states, the two capacitors- boost capacitor and dc-link capacitor are both connected in series during FEM and FDM if the outgoing phase and incoming phase currents are not overlapped in the commutation region. On another hand, if the phase currents overlap in the commutation region, the phase voltages are determined by the relationship of the overlapping currents. The demagnetization voltage of the outgoing phase is equal to the excitation voltage of the incoming phase during current overlap.

Fig. 6 shows the phase voltage and current waveforms of the NBC under angle position control (APC). According to the turn-on position of the incoming phase, there are two cases for the current overlap operation, as shown in Fig. 6(a) and (b). In case 1, $15°\le\theta_{off\_A}\le\theta_{on\_B}$, during the first period of the current overlap of two phases, before the FDM of the outgoing phase is ended, the incoming phase-B is turned on (S_b is also turned on), the outgoing phase-A and the incoming phase-B are in state 4. After S_b is turned off, the outgoing phase-A and the incoming phase-B are in state 5. In case 2, $\theta_{off\_A}\le\theta_{on\_B}<15°$, during the current overlap of two phases, the outgoing phase-A and the incoming phase-B are in state 4 until the fast demagnetization current of the outgoing phase-A is reduced to zero.

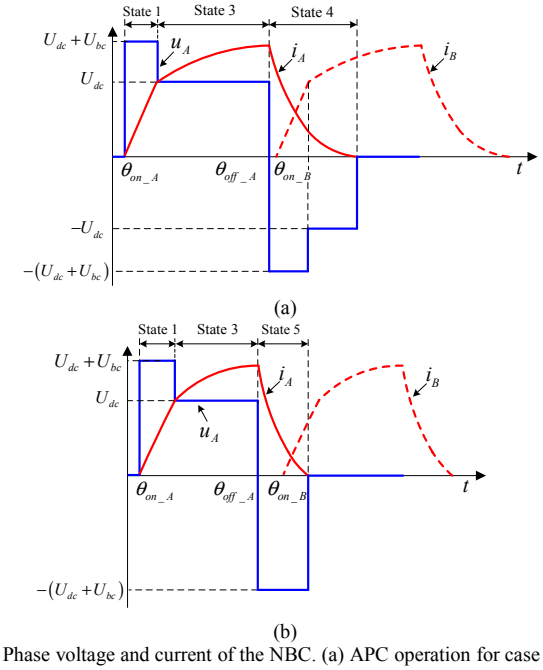

Fig. 6. Phase voltage and current of the NBC. (a) APC operation for case 1. (b) APC operation for case 2.

C. *Dynamic Performance and Comparison with AHBC*

Fig. 7 shows the simulated results of the SSHE-SRM driven by two converters (NBC and AHBC) under APC mode at 900r/min. In this case, the dc-link voltage is 110V and the turn-on and turn-off angles are fixed at 0° and 15°, respectively. As can be seen from Fig. 7, a higher voltage is applied in the periods of excitation and demagnetization for the NBC due to the addition of the capacitor voltage. During the current overlap of two phases, there are two states (4 and 5) for the outgoing phase, which is quite consistent with the analysis in Fig. 6(a). The phase current and output torque with the NBC are higher than those with AHBC.

Fig. 8 shows the simulated results of the SSHE-SRM driven by two converters under APC mode at 1500r/min. In this case, the dc-link voltage is 150V and the turn-on and turn-off angles are fixed at 0° and 12°, respectively. As can be seen from Fig. 8, a higher voltage is also applied in the periods of excitation and demagnetization for the NBC due to the addition of the capacitor voltage. However, there is only one state (4) for the outgoing phase during the current overlap of two phases, which is also quite consistent with the analysis in Fig. 6(b). The phase current and output torque with the NBC are also higher than those with AHBC.

Finally, Table I summarizes the predicted performances of the SSHE-SRM based on the NBC and AHBC at different conditions and control modes. As shown in Table I, the characteristic of the SSHE-SRM based on NBC is better than that based on AHBC, such as higher average torque, lower torque ripple and higher torque density under the same conditions.

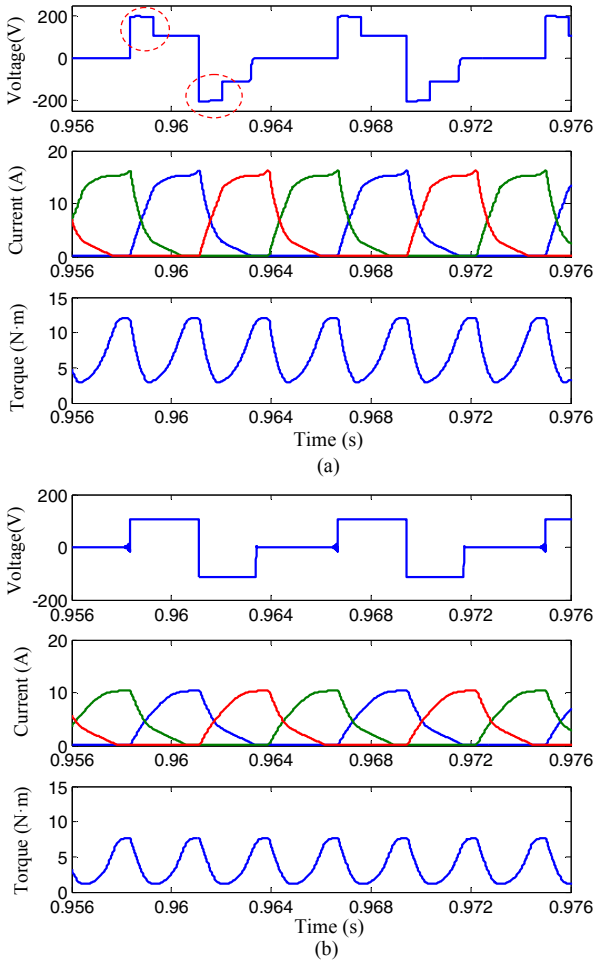

Fig. 7. Steady-state performances of two converters with APC mode at 900rpm, θ_{ON}=0°, θ_{OFF}=15°. (a) Proposed NBC. (b) AHBC.

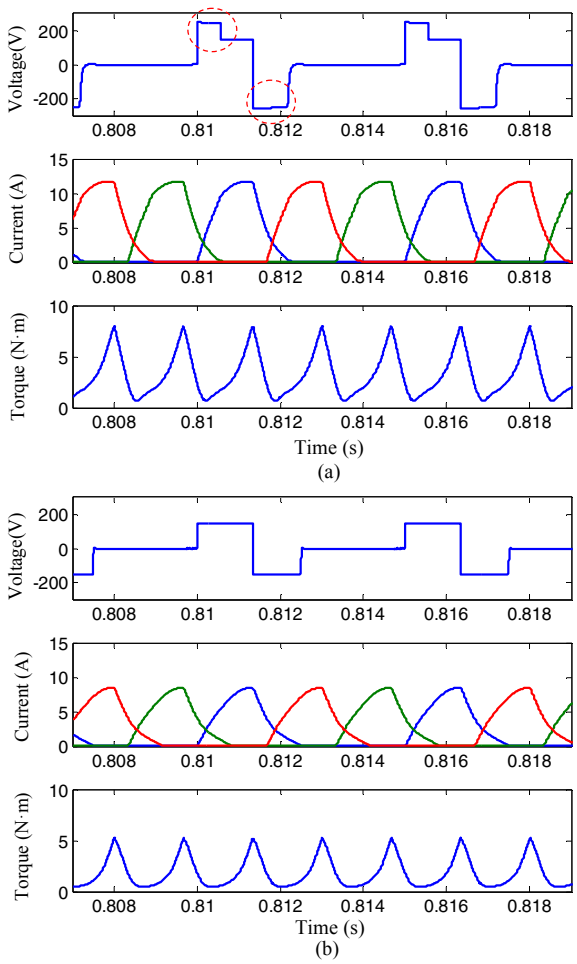

Fig. 8. Steady-state performances of two converters with APC mode at 1500rpm, θ_{ON}=0°, θ_{OFF}=12°. (a) Proposed NBC. (b) AHBC.

Table I The summary of predicted performances of two converters.

Power converter	NBC		AHBC	
Control mode	APC	APC	APC	APC
Speed, r/min	900	1500	900	1500
DC-link voltage, V	110	150	110	150
RMS phase current, A	7.72	6.72	5.15	3.63
Average torque, N·m	6.77	4.66	3.96	1.91
Torque per ampere, N·m/A	0.88	0.69	0.77	0.58
Torque ripple, %	133	225	167	256
Torque density, N·m/kg	1.52	1.04	0.89	0.43
Output power, W	637.7	731.6	373.0	307.7
Copper loss, W	219.9	166.6	97.9	48.6
Copper loss per torque, W/N·m	32.5	35.8	24.7	25.5

IV. Experimental Verification

In order to validate above theoretical analysis, predictions and simulations of dynamic performance, a 12/8 SSHE-SRM prototype is manufactured and the SSHE-SRM drive with NBC and AHBC is developed for experimentally test. Fig. 9 shows detailed photographs of the 12/8 SSHE-SRM prototype.

The static flux linkage and average torque characteristics of the SSHE-SRM are tested and validated. In order to measure the static magnetic characteristics, a simple indirect method, namely locked-rotor test, is performed. The measured results of the SSHE-SRM with FEA results are compared and shown in Fig. 10. It can be seen that the FEA result agrees well with the measured values, which validates aforementioned analysis. The errors may be attributable to the neglect of end effect in 2D-FEA, nonuniformity of the air gap and manufacturing tolerances.

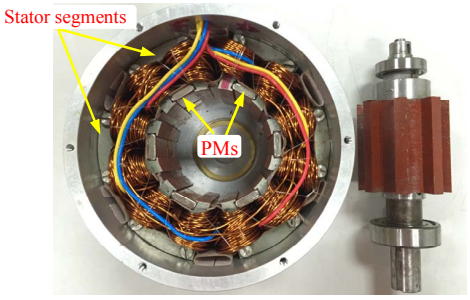

(a) (b)

Fig. 9. Photographs of 12/8 SSHE-SRM prototype. (b) Stator. (b) Rotor.

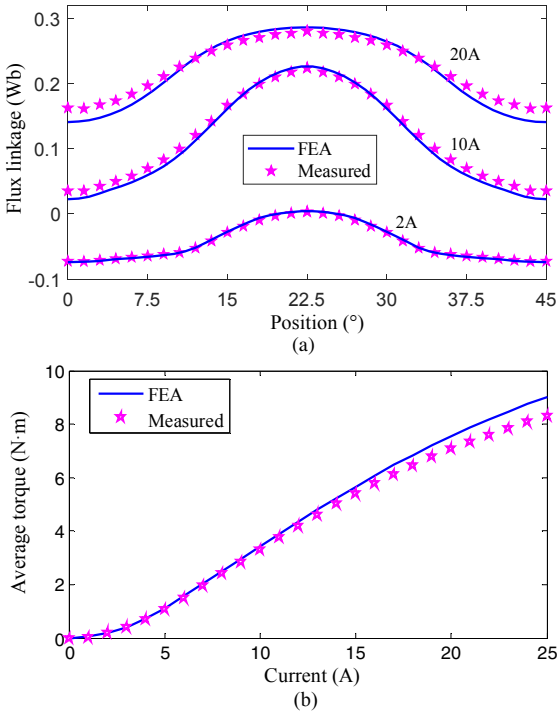

Fig. 10. Static characteristics of the SSHE-SRM obtained from FEA and measurement. (a) Flux linkage. (b) Static average torque.

A steady-state operation driven by two converters with APC mode is experimentally tested, as shown in Fig. 11. In this case, the dc-link voltage is 110V, the speed is 1000r/min, the turn-on and turn-off angles are 0° and 15°, respectively. It can be seen from Fig. 11 that a larger voltage is exerted with the NBC in the period of excitation and demagnetization. There are two states (4 and 5) for the outgoing phase during the current overlap of two phases, which is quite consistent with the analysis in Fig. 6(a). The fast excitation and

demagnetization times are only 0.85ms and 1.08ms in the NBC, which are shorter than those in the AHBC. A detailed comparison between the measured results is listed in Table II. The output torque using the NBC is higher than that using AHBC by 67%. The values of torque per ampere and torque density of the former are both larger than the latter.

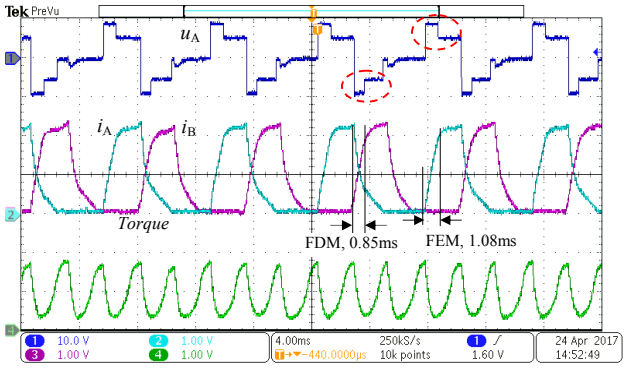

(a)

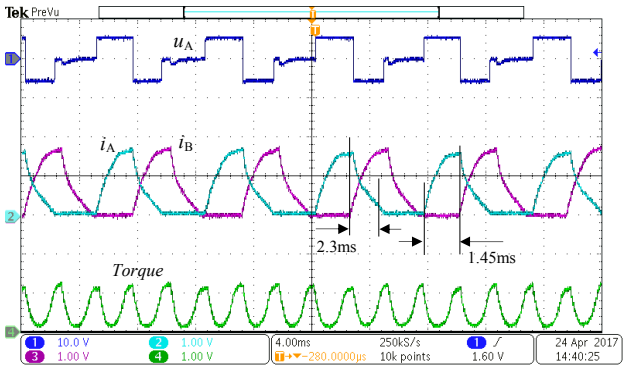

(b)

Fig. 11. Comparison of experimental results of two converters with APC mode at 1000r/min. (a) NBC. (b) AHBC. (CH1: phase voltage, 200V/div; CH2, CH3: phase currents, 5A/div; CH4: torque, 5N·m/div).

TABLE II MEASURED RESULTS WITH DIFFERENT CONVERTERS AT 110V, 1000r/min, θ_{ON}=0° AND θ_{OFF}=15°

	NBC	AHBC	Percentage of difference
RMS Phase current, A	6.05	4.45	36%
Average torque, N·m	5.02	3.0	67%
Torque per ampere, N·m/A	0.83	0.65	26%
Torque density, N·m/kg	1.12	0.67	67%
Output power, W	525.4	314	67%
Copper loss per torque, W/N·m	26.9	25.8	4%

V. CONCLUSION

In this paper, a novel boost converter is proposed and investigated for a three-phase 12/8-pole SSHE-SRM drive to improve its dynamic performance. The operation states of the SSHE-SRM with the NBC are analyzed in detail. Higher voltage is applied to phase windings and fast excitation and fast demagnetization currents are obtained owing to the addition of the capacitor voltage. Simulations of the SSHE-SRM drive based on the NBC are carried out as well as compared with AHBC. The simulation result demonstrates that the SSHE-SRM drive with the NBC has better dynamic characteristic than that with AHBC, such as higher average torque, higher torque density, and higher output power capability, etc. A 12/8 SSHE-SRM is prototyped and tested. The experimental results of static magnetic characteristics, steady state and transient performances with the NBC and AHBC have been presented to validate the analysis and conclusions.

REFERENCES

[1] L. Szabó, and M. Ruba, "Segmental stator switched reluctance machine for safety-critical applications," *IEEE Trans. Ind. Applicat.*, vol. 48, no. 6, pp. 2223-1229, Nov/Dec. 2012.

[2] A. Labak, and N. C. Kar, "Designing and prototyping a novel five-phase pancake-shaped axial-flux SRM for electric vehicle application through dynamic FEA incorporating flux-tube modeling," *IEEE Trans. Ind. Applicat.*, vol. 49, no. 3, pp. 1276-1288, May/June. 2013.

[3] C. Lee, R. Krishnan, and N. S. Lobo, "Novel two-phase switched reluctance machine using common-pole E-core structure: Concept, analysis, and experimental verification," *IEEE Trans. Ind. Appl.*, vol. 45, no. 2, pp. 703–711, Mar./Apr. 2009.

[4] J. Liang, D. H. Lee, G. Q. Xu, and J. W. Ahn, "Analysis of passive boost power converter for three-phase SR drive," *IEEE Trans. Ind. Electro*, vol. 57, no. 9, pp. 2961-2971, Sep. 2010.

[5] D. H. Lee, and J. W. Ahn, "A novel four-level converter and instantaneous switching angle detector for high speed SRM drive," *IEEE Trans. Pow. Electro*, vol. 22, no. 5, pp. 2034-2041, Sep. 2007.

[6] R. Krishnan and P. N. Materu, "Design of a single-switch-per-phase converter for switched reluctance motor drives," *IEEE Trans. Ind. Electron.*, vol. 37, no. 6, pp. 469–476, Dec. 1990.

[7] K. Tomczewski and K. Wrobel, "Improved C-dump converter for Switched reluctance motor drives", *IET Power Electronics*, Vol. 7, no. 10, pp. 2628-2635, Oct. 2014.

[8] J. Kim and R. Krishnan, "Novel two switch based SRM drive for low cost high volume applications", *IEEE Trans. Ind. Appl.,*vol. 45, no. 4, pp.1241-1248, Aug. 2009.

[9] Y. Hasegawa, K. Nakamura, and O. Ichinokura, "A novel switched reluctance motor with the auxiliary windings and permanent magnets," *IEEE Trans. Magn.*, vol. 48, no. 11, pp. 5574-5589, Nov. 2012.

[10]K. Nakamura and O. Ichinokura, "Super-multipolar permanent magnet reluctance generator designed for small-scale wind-turbine generation," *IEEE Trans. Magn.*, vol. 48, no. 11, pp. 3311-3314, Nov. 2012.

[11]K. Y. Lu, U. Jakobsen, and P. O. Rasmussen, "Single-phase hybrid switched reluctance motor for low-power low-cost applications," *IEEE Trans. Magn.*, vol. 47, no. 10, pp. 3288-3291, Oct. 2011.

[12]K. Nakamura, E. Sunan, O. Ichinokura, "Development of 72/96-pole rareearth free permanent magnet reluctance generator for small-scale renewable power generation," *IEEJ Jour. Ind. Applicat.*, vol. 3, no. 1, pp. 41-46, 2014.

[13]P. Andrada, B. Blanqué, E. Martínez, and M. Torrent, "A novel type of hybrid reluctance motor drive," *IEEE Trans. Ind. Electro*, vol. 61, no. 8, pp. 4337-4345, Aug. 2014.